Mathematical Sciences Letters
An International Journal

http://dx.doi.org/10.12785/msl/040302

On the Numerical Simulation of Schnakenberg Model on Evolving Surface

Mahdieh Sattari * *and Jukka Tuomela*

University of Eastern Finland, Department of Physics and Mathematics, P.O. Box 111, FI-80101 Joensuu, Finland

Received: 3 Mar. 2015, Revised: 19 May 2015, Accepted: 25 May 2015
Published online: 1 Sep. 2015

Abstract: The Schnakenberg model can be used to describe the emergence of patterns on the animal skin. The problem is numerically challenging for two reasons. First the organism grows so the computational domain changes. Second the domain is topologically a sphere and hence cannot be considered as a subset of the plane. In our approach we consider the computational domain as a sphere whose Riemannian metric changes and use special parametrization of the sphere to formulate the discrete problem. Our choice of parametrization allows a very convenient way to treat a large class of surfaces in a straightforward way and in a similar way one could treat other PDE systems on surfaces. The same kind of ideas can be used also to compute on surfaces which are not diffeomorphic to a sphere. We have used finite elements in the discretization. We have also analyzed how the eigenfunctions of the Laplacian are related to the emergence of patterns.

Keywords: Schnakenberg model, finite elements, evolving surface

1 Introduction

The models describing the emergence of patterns have a long history which can be traced at least back to Turing's work on diffusion driven instability. The basic reference on the applications to biology is [1]. In recent years there has been a lot of interest on these questions from the numerical point of view, see [2,3,4,5,6,7] and references therein. The models are quite challenging numerically. Typically they are nonlinear so that even basic existence and uniqueness results may be unavailable. Also in biological and other contexts the computational domain is not fixed but evolves with time. Finally if the patterns are on the skin of the animal then it is most reasonable to consider the domain as a two dimensional manifold without boundary.

Due to the numerical difficulties the actual computations in [1] were carried out in flat domains with homogeneous Neumann boundary conditions. In this situation one obviously hopes that the solution in the interior would be "qualitatively correct" although near boundaries it is more or less arbitrary.

To compute the solution on some surface there are two basic possibilities: either one considers the surface as a submanifold of $\mathbb{R}^3$ and then one tries to approximate it there, or one parametrizes the surface so that all computations are reduced to parameter domain. There are some advantages and disadvantages in both approaches. When the surface is considered as a submanifold of $\mathbb{R}^3$ one can treat it "globally" but one necessarily has an extra source of error because in essence one replaces the surface by an approximation. When one parametrizes the surface there is no error of approximation but on the other hand one must explicitly construct the parametrization maps. In addition one parameter domain is never enough and one must somehow put together different parameter domains.

In this article we consider the second possibility. In biological applications for the emergence of patterns the surface is a topological sphere which evolves over time. However, since the topological type of the surface does not change we can consider it as a fixed sphere whose Riemannian metric changes. Hence we can apply here the same ideas that were already used in [8,9]. The change in the Riemannian metric can be sometimes interpreted as a kind of moving grid method. This idea is developed in the present context for example in [10]. However, the analogy is strictly speaking valid only when one considers two dimensional domains in $\mathbb{R}^2$. When one considers surfaces then the moving grids are constructed in $\mathbb{R}^3$ and at most

* Corresponding author e-mail: mahdieh.sattari@uef.fi

one can say that in some situations it is possible that on the numerical level the moving grid method could be close to our approach. Note also that on the practical level one should take care that the mesh tangling is avoided in the moving grid method. However, in our method such problems cannot arise.

One contribution of our paper is that in this framework we can quite easily do simulations on quite a large class of surfaces. It would even be possible to incorporate realistic shapes of animals in this framework. The second contribution is to analyze more precisely the role of the eigenfunctions of the Laplacian on the surface. It appears that at least in certain situations the emerging patterns can be qualitatively predicted by analyzing the eigenvalues and the eigenfunctions of the Laplacian. As far as we know this property has not been observed before, perhaps because the round sphere is the most common example and this has a very atypical structure of eigenvalues.

In this paper we use the well known Schnakenberg model [11] to study the emergence of patterns and we have implemented our method when the evolving surface is topologically a sphere. However, our approach can also be adapted to other types surfaces. Also our code can easily be adapted to other diffusion type models.

The structure of the article is as follows. First in section 2 we recall some necessary background from differential geometry. In section 3 we introduce the Schnakenberg model first in the standard 2 dimensional domain and recall some of the properties of the model. Then we formulate the model on arbitrary compact time dependent manifold. In section 4 we show how to use finite elements and method of lines to solve numerically the resulting system. We also show how in this context one can conveniently define time dependent families of surfaces. In section 5 we give several numerical results and finally in section 6 we give some general conclusions.

2 Preliminaries

We start by recalling some facts from differential geometry. More details can be found in [12].

2.1 Riemannian geometry

Let g be a Riemannian metric on some smooth orientable manifold $\mathscr{S}$ with (possibly empty) boundary $\partial\mathscr{S}$. The components of g in the coordinate system are denoted by g_{ij}, and the resulting matrix is G. The components of G^{-1} are denoted by g^{ij}. The canonical volume form of $\mathscr{S}$ is denoted by $\omega_{\mathscr{S}}$ and the corresponding volume by $\mathrm{vol}(\mathscr{S})$ or $\mathrm{vol}_g(\mathscr{S})$. The induced volume form on $\partial\mathscr{S}$ is denoted by $\omega_{\partial\mathscr{S}}$.

Then if w is some vector field on $\mathscr{S}$ we can define the gradient of u by the formula

$$g(\mathrm{grad}(u), w) = du\, w = w(u)$$

The standard gradient (resp. divergence and Laplacian) operator in Euclidean spaces is denoted by ∇ (resp. $\nabla\cdot$ and Δ) as usual. In a coordinate system we can write

$$\mathrm{grad}(u) = G^{-1}\nabla u = \sum_{i=1}^{n}\sum_{j=1}^{n} g^{ij}\frac{\partial u}{\partial x_j}\frac{\partial}{\partial x_i}$$

$$g(\mathrm{grad}(u), \mathrm{grad}(v)) = \langle \nabla u, G^{-1}\nabla v\rangle$$

The divergence of a vector field $w = \sum_i w_i \partial/\partial x_i$ is given in coordinates by

$$\mathrm{div}(w) = \frac{1}{\sqrt{\det(G)}}\sum_i \frac{\partial}{\partial x_i}\left(\sqrt{\det(G)}\, w_i\right)$$

Finally the Laplacian of u is given by $\Delta_{\mathscr{S}} u = \mathrm{div}\big(\mathrm{grad}(u)\big)$ and the coordinate expression is obtained by combining the formulas for divergence and gradient. However, the coordinate formulas for Laplacian and divergence are not in fact needed in our computations.

The divergence theorem is valid also for general Riemannian manifolds.

Theorem 2.1. Let $\mathscr{S}$ be a compact Riemannian manifold, w a vector field on $\mathscr{S}$ and ν the outer unit normal field of the boundary $\partial\mathscr{S}$. Then

$$\int_{\mathscr{S}} \mathrm{div}(w)\omega_{\mathscr{S}} = \int_{\partial\mathscr{S}} g(w,\nu)\omega_{\partial\mathscr{S}}$$

If $\mathscr{S}$ is a manifold without boundary the right hand side of the above formula vanishes. The following formulas follow immediately. If u and v are functions and w is a vector field then

$$\int_{\mathscr{S}} v\Delta_{\mathscr{S}} u\,\omega_{\mathscr{S}} + \int_{\mathscr{S}} g(\mathrm{grad}(u),\mathrm{grad}(v))\,\omega_{\mathscr{S}} = \int_{\partial\mathscr{S}} v\, g(\mathrm{grad}(u),\nu)\,\omega_{\partial\mathscr{S}}$$

$$\int_{\mathscr{S}} g(\mathrm{grad}(u), w)\omega_{\mathscr{S}} + \int_{\mathscr{S}} u\,\mathrm{div}(w)\omega_{\mathscr{S}} = \int_{\partial\mathscr{S}} u\, g(w,\nu)\,\omega_{\partial\mathscr{S}}$$

One can define the usual Sobolev spaces on $\mathscr{S}$ using local charts and the above formulas are thus valid for same spaces as in the case where $\mathscr{S}$ is a domain in $\mathbb{R}^n$.

2.2 Growth, eigenvalues and eigenfunctions

Let $\mathscr{S}$ be a compact manifold without boundary and let us denote the eigenvalues of $-\Delta_{\mathscr{S}}$ by λ_k or $\lambda_k(g)$ if needed. Recall that $\lambda_0 = 0 < \lambda_1 \le \lambda_2 \le \dots$ and that $\lambda_k \to \infty$ when $k \to \infty$. It is also convenient sometimes to write eigenvalues without multiplicities in which case we write $\hat\lambda_0 = 0 < \hat\lambda_1 < \hat\lambda_2 < \dots$. For the unit sphere with

standard metric the eigenvalues (and even the eigenfunctions) are known and we have

$$\begin{cases} \hat{\lambda}_k = k(k+1) \\ m_k = 2k+1 \end{cases} \tag{1}$$

Here m_k are the corresponding multiplicities. If we scale the metric by $g_\mu = \mu g$ then the volume scales as $\mathrm{vol}_{g_\mu}(\mathscr{S}) = \mu^{n/2}\mathrm{vol}_g(\mathscr{S})$ where n is the dimension of $\mathscr{S}$. Also the minimax characterization of the eigenvalues readily implies that

$$\lambda_k(g_\mu) = \frac{\lambda_k(g)}{\mu} \tag{2}$$

In case $\mathscr{S}$ is embedded in some $\mathbb{R}^N$ then we obtain the same effect by scaling the embedding linearly by $\sqrt{\mu}$.

Let us then denote by S^2 any smooth surface which is diffeomorphic to the standard sphere. We have the following interesting estimate for the smallest eigenvalues of the laplacian on such surfaces [13, p. 410].

Theorem 2.2.

$$\frac{1}{\lambda_1} + \frac{1}{\lambda_2} + \frac{1}{\lambda_3} \geq \frac{3\,\mathrm{vol}_g(S^2)}{8\pi}$$

The equality is attained only for the standard round metric. In particular

$$\lambda_1(g_\mu) \leq \frac{8\pi}{\mathrm{vol}_{g_\mu}(S^2)} = \frac{8\pi}{\mu\,\mathrm{vol}_g(S^2)} \tag{3}$$

Finally recall that the eigenfunctions are orthogonal in the sense that if u_k and u_ℓ are two different eigenfunctions of $-\Delta_{\mathscr{S}}$ then

$$\int_{\mathscr{S}} u_k\, u_\ell\, \omega_{\mathscr{S}} = 0 \tag{4}$$

2.3 Balance laws

Let us consider a family of Riemannian manifolds $\mathscr{S}_t$ such that they are all diffeomorphic to some fixed manifold $\mathscr{S}$. Let us further denote by $\Phi_t : \mathscr{S} \to \mathscr{S}_t$ the corresponding diffeomorphisms. We denote by g^t the Riemannian metric of $\mathscr{S}_t$ and by $\omega_{\mathscr{S}_t}$ the corresponding volume form.

Let then $\mathscr{U} \subset \mathscr{S}$ and $\Phi_t(\mathscr{U}) = \mathscr{U}_t \subset \mathscr{S}_t$. Suppose now that for all $\mathscr{U}_t$ we have

$$\frac{d}{dt}\int_{\mathscr{U}_t} a\,\omega_{\mathscr{S}_t} = \int_{\mathscr{U}_t} b\,\omega_{\mathscr{S}_t} + \int_{\partial\mathscr{U}_t} g_t(v,v)\omega_{\partial\mathscr{U}_t}$$

where a, b are some functions and v is a vector field. This is called the *master balance law* in [14]. Using the divergence theorem 2.1 we write this as

$$\frac{d}{dt}\int_{\mathscr{U}_t} a\,\omega_{\mathscr{S}_t} = \int_{\mathscr{U}_t} \Big(b + \mathrm{div}(v)\Big)\,\omega_{\mathscr{S}_t}$$

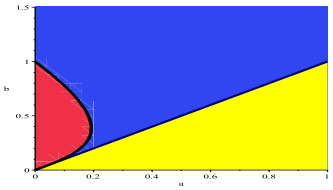

Fig. 1: The system (6) can have diffusion driven instability only if (a,b) is in the blue region.

Then using Φ_t and setting $J^t = \det(d\Phi^t)$ we obtain the corresponding formula on $\mathscr{S}$:

$$\frac{d}{dt}\int_{\mathscr{U}} a\,J^t\,\omega_{\mathscr{S}} = \int_{\mathscr{U}} \Big(b + \mathrm{div}(v)\Big)\,J^t\,\omega_{\mathscr{S}}$$

But since $\mathscr{U}$ is arbitrary this implies that

$$\partial_t\big(a\,J^t\big) = \Big(b + \mathrm{div}(v)\Big)\,J^t \tag{5}$$

Our model and the numerical computations will be based on this equation and the corresponding variational formulation.

3 Schnakenberg model

3.1 Standard setting

Let us first recall the formulation of the *Schnakenberg model* in a standard setting. Let $\Omega \subset \mathbb{R}^2$ be some domain and let $u : \Omega \to \mathbb{R}^2$. The model is given by

$$\begin{aligned} \partial_t u_1 - d_1\Delta u_1 &= \gamma(a - u_1 + u_1^2 u_2) \\ \partial_t u_2 - d_2\Delta u_2 &= \gamma(b - u_1^2 u_2) \end{aligned} \tag{6}$$

where d_j, a, b and γ are some positive constants. As boundary conditions one typically takes homogeneous Neumann boundary conditions. It is also useful to consider the corresponding stationary problem

$$\begin{aligned} -d_1\Delta u_1 &= \gamma(a - u_1 + u_1^2 u_2) \\ -d_2\Delta u_2 &= \gamma(b - u_1^2 u_2) \end{aligned} \tag{7}$$

We are only interested in nonnegative solutions. Note that the model admits the constant solution

$$u = \Big(a + b, \frac{b}{(a+b)^2}\Big) \tag{8}$$

Let us then summarize the reasons for choosing certain values for parameters. For an extensive discussion and background on this we refer to [1]. In diffusion driven instability we first choose a and b so that without diffusion the equilibrium solution given by (8) is stable.

This gives the condition (indicated by the blue region in Figure 1)

$$(a+b)^3+a-b>0 \quad \text{and} \quad a<b$$

Next we must choose diffusion parameters such that linear stability analysis shows some unstable modes. This gives the necessary condition

$$\sqrt{\frac{d_2}{d_1}} > \frac{(a+b)\left(a+b+\sqrt{2b(a+b)}\right)}{b-a}$$

In particular $d_2 > d_1$. Consider now the polynomial

$$p_0(y) = d_1 d_2 (a+b) y^2 + \Big((a+b)^3 d_1 + (a-b) d_2\Big) y + (a+b)^3$$

If the parameters are chosen as indicated above this polynomial has 2 positive roots, denoted by $y_{\min}$ and $y_{\max}$. We call the interval $I_{\text{crit}} = (y_{\min}, y_{\max})$ the *critical interval*. Then consider the polynomial

$$p_1(\mu, y) = (a+b)\mu^2 + p_0(y) + \Big((d_1+d_2)(a+b)y + (a+b)^3 + a - b\Big)\mu$$

Suppose that λ is an eigenvalue of $-\Delta$ and let v_λ be the corresponding eigenfunction. If $\lambda/\gamma \in I_{\text{crit}}$ then $p_1(\mu, \lambda/\gamma)$, considered as a polynomial in μ, has a positive root, denoted by μ_+. In this case the linearized problem has an exponentially growing solution of the form $c\, v_\lambda(x) \exp(\gamma \mu_+ t)$ where $c \in \mathbb{R}^2$.

Note that this analysis shows that the parameter γ is in a sense superfluous: the scaling of γ has the same effect on (in)stability as scaling the domain, see (2).

3.2 Some (in)existence results

Let us recall some results from [15]. We consider the model (6) with homogeneous Neumann boundary condition and with appropriate nonnegative initial condition. Then we have

Theorem 3.1. The system (6) has at least one solution which is smooth, bounded and global in time.

Now when modelling for patterns one expects that the solution would tend to a stationary solution which is not the constant solution (8). Hence there should be more than one solution to the stationary problem (7). However, there is the following result.

Theorem 3.2. There is a positive constant c such that (7) has no nonconstant solutions, if $\lambda_1 > c$.

Recall that eigenvalues scale as in (2). This implies that if the domain is too small there can be no stable patterns. Note that this does not necessarily mean that the solution (8) is stable. The model could still in principle have oscillating solutions which do not tend to a definite limit. Anyway for the emergence of patterns it is thus necessary that the constant solution is unstable and that the domain is big enough. In other words the growth of the domain really seems to be essential in the emergence of patterns.

3.3 Changing manifold

In the biological context a flat domain in $\mathbb{R}^2$ is not very realistic. If the goal is to analyse the patterns on the skin it is more natural to consider the problem on a compact surface without boundary. It seems that all the examples that are found in the literature are of the following form.

Definition 3.1. A family of surfaces $\mathscr{S}_t$ with Riemannian metric g^t is *nice*, if there are maps Φ_t and the surface $\mathscr{S}$ with following properties:

(i) $\Phi_t : \mathscr{S} \to \mathscr{S}_t$ is diffeomorphism for all $t \geq 0$.
(ii) the map Φ defined by $\Phi(t,x) = \Phi_t(x)$ is smooth.
(iii) the limit $\mathscr{S}_\infty = \lim_{t\to\infty} \mathscr{S}_t$ is well defined and $\mathscr{S}_\infty$ is diffeomorphic to $\mathscr{S}$.
(iv) the limit $g^\infty = \lim_{t\to\infty} g^t$ is well defined and g^∞ is a Riemannian metric on $\mathscr{S}_\infty$.

The surface $\mathscr{S}_0$ is called the *initial surface* (or initial shape) and $\mathscr{S}_\infty$ is called the *final surface* (or final shape). Note that Φ is "almost" an isotopy between $\mathscr{S}_0$ and $\mathscr{S}_\infty$. However, in the present context it is more convenient to consider the infinite interval $[0,\infty)$ instead of some bounded interval as in the usual definition.

Definition 3.2. *Schnakenberg model* on a nice family of surfaces is the system

$$\begin{aligned} \partial_t(J^t u_1) - d_1 J^t \Delta_{\mathscr{S}} u_1 &= \gamma(a - u_1 + u_1^2 u_2) J^t = f_1 J^t \\ \partial_t(J^t u_2) - d_2 J^t \Delta_{\mathscr{S}} u_2 &= \gamma(b - u_1^2 u_2) J^t = f_2 J^t \end{aligned} \tag{9}$$

Here we have combined the balance law (5) and the standard Schnakenberg's model (6). We are not aware of any rigorous existence and uniqueness results for the system (9) in Sobolev spaces. However, in [16] there are some results for similar systems. The functions u_i are defined on $\mathscr{S}$ and the corresponding functions on $\mathscr{S}_t$ are given by $u_i^t(x,t) = u_i\big(\Phi_t^{-1}(x), t\big)$.

Note that the constant solution (8) is *not* a solution of the system (9) because J^t is not constant. However, since g^∞ is well defined there is also some $J^\infty = \lim_{t\to\infty} J^t$. Hence it is still quite possible that in some situations the solution tends asymptotically to (8). However, when studying the emergence of patterns one is naturally interested in stationary solutions which are not constant.

4 Numerical model

4.1 Variational formulation

Our goal is to solve the model (9). Let $\psi : \mathscr{S} \to \mathbb{R}$ be some function and let $\psi^t(x) = \psi\big(\Phi_t^{-1}(x)\big)$. Then we have

$$\int_{\mathscr{S}} \Big(\partial_t(J^t u_i) - d_i J^t \Delta_{\mathscr{S}} u_i\Big)\psi\,\omega_{\mathscr{S}} =$$
$$\partial_t \int_{\mathscr{S}} u_i \psi J^t \omega_{\mathscr{S}} + d_i \int_{\mathscr{S}} g(\mathrm{grad}(u_i), \mathrm{grad}(\psi)) J^t\,\omega_{\mathscr{S}} =$$
$$\partial_t \int_{\mathscr{S}_t} u_i^t \psi^t\,\omega_{\mathscr{S}_t} + d_i \int_{\mathscr{S}_t} g^t(\mathrm{grad}(u_i^t), \mathrm{grad}(\psi^t))\,\omega_{\mathscr{S}_t} =$$
$$\int_{\mathscr{S}_t} f_i^t \psi^t\,\omega_{\mathscr{S}_t}$$

This is the basis of our numerical computations. Let us now proceed in the context of finite element methods. Let V_h be some finite dimensional space of functions defined on $\mathscr{S}$:

$$V_h = \mathrm{span}\big\{\psi_1, \ldots, \psi_m\big\} \tag{10}$$

Let us first look for the approximate solution of the form $u_h = (u_{1,h}, u_{2,h})$ where

$$u_{i,h}(x,t) = \sum_{j=1}^{m} c_j^i(t)\psi_j(x) \approx u_i(x,t)$$

This leads to the following semi discrete variational formulation:

(V) *find* $(u_{1,h}, u_{2,h})$ *of the above form such that for all* $1 \le j \le m$

$$\partial_t \int_{\mathscr{S}_t} u_{1,h}^t \psi_j^t \omega_{\mathscr{S}_t} + d_1 \int_{\mathscr{S}_t} g^t(\mathrm{grad}(u_{1,h}^t), \mathrm{grad}(\psi_j^t))\omega_{\mathscr{S}_t} =$$
$$\int_{\mathscr{S}_t} f_1^t \psi_j^t \omega_{\mathscr{S}_t}$$
$$\partial_t \int_{\mathscr{S}_t} u_{2,h}^t \psi_j^t \omega_{\mathscr{S}_t} + d_2 \int_{\mathscr{S}_t} g^t(\mathrm{grad}(u_{2,h}^t), \mathrm{grad}(\psi_j^t))\omega_{\mathscr{S}_t} =$$
$$\int_{\mathscr{S}_t} f_2^t \psi_j^t \omega_{\mathscr{S}_t}$$

To obtain a more convenient formulation we introduce the following (time dependent) matrices and tensors:

$$M_{ij}(t) = \int_{\mathscr{S}_t} \psi_i^t \psi_j^t \omega_{\mathscr{S}_t}$$
$$R_{ij}(t) = \int_{\mathscr{S}_t} g^t(\mathrm{grad}(\psi_i^t), \mathrm{grad}(\psi_j^t))\omega_{\mathscr{S}_t}$$
$$E_{ijk\ell}(t) = \int_{\mathscr{S}_t} \psi_i^t \psi_j^t \psi_k^t \psi_\ell^t \omega_{\mathscr{S}_t}$$
$$F_i(t) = \int_{\mathscr{S}_t} \psi_i^t \omega_{\mathscr{S}_t}$$
$$\tilde{M}_{ij}(t) = \sum_{k,\ell} E_{ijk\ell}(t) c_k^1(t) c_\ell^2(t)$$
$$\hat{M}_{ij}(t) = \sum_{k,\ell} E_{ijk\ell}(t) c_k^1(t) c_\ell^1(t)$$

Evidently M (resp. R) is symmetric and positive definite (resp. positive semidefinite). Also E, $\tilde{M}$ and $\hat{M}$ are symmetric and we have

Lemma 1. *E and $\hat{M}$ are positive definite. $\tilde{M}$ is positive definite, if the approximations $u_{1,h}$ and $u_{2,h}$ are positive.*

Proof. Let $\alpha \in \mathbb{R}^m$ and $v = \sum_i \alpha_i \psi_i$. Then

$$\langle \alpha, \hat{M}\alpha \rangle = \int_{\mathscr{S}} (v^t)^2 \big(u_{1,h}^t\big)^2 \omega_{\mathscr{S}_t} > 0$$

Similarly

$$\langle \alpha, \tilde{M}\alpha \rangle = \int_{\mathscr{S}_t} (v^t)^2 u_{1,h}^t u_{2,h}^t \omega_{\mathscr{S}_t} > 0$$

if $u_{1,h} > 0$ and $u_{2,h} > 0$. E is said to be positive definite if $\sum_{ijk\ell} E_{ijk\ell} A_{ij} A_{k\ell} > 0$ for all symmetric nonzero matrices A. Let λ_s, $1 \le s \le m$, be the eigenvalues of A and let w^s be the corresponding eigenvectors. Let $v_s = \sum_i w_i^s \psi_i$. Then

$$\sum_{ijk\ell} E_{ijk\ell} A_{ij} A_{k\ell} = \int_{\mathscr{S}_t} \Big(\sum_s \lambda_s (v_s^t)^2\Big)^2 \omega_{\mathscr{S}_t} > 0$$

One could say that $\tilde{M}$ is "only" conditionally positive definite in the sense that this property depends on the fact that the solution stays positive while the positive deifiniteness of $\hat{M}$ and E does not depend on this. Note that if the approximate solution does not stay positive then the numerical solution has failed so that in successful computations $\tilde{M}$ must be positive definite.

Setting now $c^j(t) = \big(c_1^j(t), \ldots, c_m^j(t)\big)$ we can now write our semidiscrete problem as

$$\partial_t\big(Mc^1\big) + d_1 Rc^1 = \gamma\big(aF - Mc^1 + \tilde{M}c^1\big)$$
$$\partial_t\big(Mc^2\big) + d_2 Rc^2 = \gamma\big(bF - \hat{M}c^2\big)$$

To obtain a fully discrete formulation we need more notation. Let δt be the time step and let the superscript n denote the approximation or the value of some quantity at time instant $n\delta t$. In particular $c_i^{j,n} \approx c_i^j(n\delta t)$ and

$$u_{j,h}^n = \sum_{i=1}^{m} c_i^{j,n} \psi_i \approx u_{j,h}(x, n\delta t) \approx u_j(x, n\delta t)$$

Now if we use implicit Euler method to solve the semidiscrete system we should solve a nonlinear algebraic system at each time step because matrices $\tilde{M}$ and $\hat{M}$ depend on the solution. To "linearize" the resulting system we use the approximations

$$\tilde{M}^{n+1} c^{1,n+1} \approx \tilde{M}^n c^{1,n+1} \quad \text{and} \quad \hat{M}^{n+1} c^{2,n+1} \approx \hat{M}^n c^{2,n+1}$$

This gives the following system

$$\Big(M^{n+1} + \delta t\,\big(\gamma M^{n+1} + d_1 R^{n+1} - \gamma\tilde{M}^n\big)\Big)c^{1,n+1} = M^n c^{1,n} + \delta t\,\gamma a F^{n+1}$$
$$\Big(M^{n+1} + \delta t\,\big(d_2 R^{n+1} + \gamma\hat{M}^n\big)\Big)c^{2,n+1} = M^n c^{2,n} + \delta t\,\gamma b F^{n+1} \tag{11}$$

The equations can be solved independently. Note that the second equation can be solved for any time step, but for the first equation we can only say that it is solvable for sufficiently small δt. Hence our fully discrete problem is well-posed for sufficiently small δt. In general, however, there is no guarantee that the numerical solution stays positive. Note finally that we do not need to construct explicitly the tensor E because we can directly compute the elements of $\tilde{M}^n$ and $\hat{M}^n$ using the formulas

$$\tilde{M}^n_{ij} = \int_{\mathscr{S}_t} \psi^t_i \psi^t_j u^{t,n}_{1,h} u^{t,n}_{2,h} \omega_{\mathscr{S}_t} \quad , \quad \hat{M}^n_{ij} = \int_{\mathscr{S}_t} \psi^t_i \psi^t_j \left(u^{t,n}_{1,h}\right)^2 \omega_{\mathscr{S}_t} \tag{12}$$

4.2 Domain Composition

To actually solve the system (11) we have to evaluate the relevant integrals which define the matrices. To this end we introduce

Definition 4.1. The maps $\varphi_\ell : D_\ell \to \mathscr{S}$, $1 \le \ell \le s$ are an *admissible parametrization* of $\mathscr{S}$ if the following properties hold:

(i)each $D_\ell \subset \mathbb{R}^2$ is open and φ_ℓ is a diffeomorphism.
(ii)$\varphi_\ell(D_\ell) \cap \varphi_k(D_k) = \emptyset$ for $\ell \neq k$
(iii)$\mathscr{S} = \overline{\cup_\ell \varphi_\ell(D_\ell)}$

Given such a system of maps, the basis (10) and a nice family of surfaces we can define the functions

$$\hat{\psi}_{i,\ell} = \psi_i \circ \varphi_\ell = \psi^t_i \circ \Phi_t \circ \varphi_\ell = \psi^t_i \circ \varphi^t_\ell$$
$$\hat{u}_{j,h,\ell} = u_{j,h} \circ \varphi_\ell = u^t_{j,h} \circ \Phi_t \circ \varphi_\ell = u^t_{j,h} \circ \varphi^t_\ell$$

Denoting the coordinates of $\mathbb{R}^2$ by z we have first

$$\begin{aligned} M_{ij} &= \int_{\mathscr{S}_t} \psi^t_i \psi^t_j \omega_{\mathscr{S}_t} = \int_{\mathscr{S}} \psi_i \psi_j \det\left(d\Phi_t\right) \omega_{\mathscr{S}} \\ &= \sum_\ell \int_{\varphi_\ell(D_\ell)} \psi_i \psi_j \det\left(d\Phi_t\right) \omega_{\mathscr{S}} \\ &= \sum_\ell \int_{D_\ell} \hat{\psi}_{i,\ell} \hat{\psi}_{j,\ell} \det\left(d\varphi^t_\ell\right) dz_1 \wedge dz_2 \end{aligned} \tag{13}$$

Let us set $\omega^t_\ell = \det\left(d\varphi^t_\ell\right) dz_1 \wedge dz_2$. Now the metric in the coordinate domains D_ℓ are given by matrices $G^t_\ell = \left(d\varphi^t_\ell\right)^T d\varphi^t_\ell$. Hence proceeding as above and using the formulas (12) we obtain

$$\begin{aligned} R_{ij} &= \int_{\mathscr{S}_t} g^t\left(\mathsf{grad}(\psi^t_i), \mathsf{grad}(\psi^t_j)\right) \omega^t_{\mathscr{S}} \\ &= \sum_\ell \int_{D_\ell} \left\langle \nabla \hat{\psi}_{i,\ell}, (G^t_\ell)^{-1} \nabla \hat{\psi}_{j,\ell} \right\rangle \omega^t_\ell \\ \tilde{M}^n_{ij} &= \sum_\ell \int_{D_\ell} \hat{\psi}_{i,\ell} \hat{\psi}_{j,\ell} \hat{u}^n_{1,h} \hat{u}^n_{2,h} \omega^t_\ell \\ \hat{M}^n_{ij} &= \sum_\ell \int_{D_\ell} \hat{\psi}_{i,\ell} \hat{\psi}_{j,\ell} \left(\hat{u}^n_{1,h}\right)^2 \omega^t_\ell \\ F_i &= \int_{\mathscr{S}_t} \psi^t_i \omega_{\mathscr{S}_t} = \sum_\ell \int_{D_\ell} \hat{\psi}_{i,\ell} \omega^t_\ell \end{aligned} \tag{14}$$

Now the computation of all terms in the fully discrete system (11) has been reduced to standard integration in Euclidean domains. Next we discuss how to construct appropriate maps φ^t_ℓ and how to choose $\hat{\psi}_{i,\ell}$.

4.3 Sphere and its triangulation

Up to now our approach has been very general in the sense that the surfaces we have considered have been quite arbitrary. Now we turn our attention to the case where the surfaces are topological spheres. Note however that the general methodology that we employ can also be used to study other types of surfaces.

Let us first consider the unit sphere. We define the parameter domains $D_1 = (-1,1) \times (-1,1)$, $D_2 = (1,3) \times (-1,1)$ and $D_3 = (-1,1) \times (1,3)$ and the corresponding maps $\varphi_\ell : D_\ell \to S^2 \subset \mathbb{R}^3$ as follows

$$\begin{aligned} &\varphi_1 = \gamma_1^{-1/2} \begin{pmatrix} z_1 \\ z_2 \\ 1 \end{pmatrix} \quad , \quad \varphi_2 = \gamma_2^{-1/2} \begin{pmatrix} 1 \\ z_2 \\ 2 - z_1 \end{pmatrix} \\ &\varphi_3 = \gamma_3^{-1/2} \begin{pmatrix} z_1 \\ 1 \\ 2 - z_2 \end{pmatrix} \quad \text{where} \\ &\gamma_1 = 1 + z_1^2 + z_2^2 \quad , \quad \gamma_2 = 1 + (z_1 - 2)^2 + z_2^2 \\ &\gamma_3 = 1 + z_1^2 + (z_2 - 2)^2 \end{aligned} \tag{15}$$

Let us further set $D_{\ell+3} = D_\ell$ and $\varphi_{\ell+3} = -\varphi_\ell$. It is easy to check that the maps $\varphi_\ell : D_\ell \to S^2$, $1 \le \ell \le 6$ give an admissible parametrization according to Definition 4.2.

Considering the images of these maps leads to the identifications of the boundaries of the parameter domains which are indicated in Figure 2. The relevant metric in the subdomains is then given by $G_\ell = d\varphi_\ell^T d\varphi_\ell$ and the area form is

$$\omega_\ell = \sqrt{\det(G_\ell)}\, dz_1 \wedge dz_2 = \gamma_\ell^{-3/2} dz_1 \wedge dz_2 \ .$$

Using the basic maps defined in (15) we can now construct more complicated topological spheres with the maps $\varphi^t_\ell = \Phi^t \circ \varphi_\ell$ by choosing a suitable time dependent map Φ^t. The corresponding matrices G^t_ℓ which give the Riemannian metric in this case are then $G^t_\ell = (d\varphi^t_\ell)^T d\varphi^t_\ell = d\varphi_\ell^T (d\Phi^t)^T d\Phi^t d\varphi_\ell$.

It remains to choose appropriate $\hat{\psi}_{i,\ell}$. We have used standard finite elements. First we triangulate each subdomain D_ℓ separately but in such a way that the triangulations are compatible on subdomain boundaries. In Figure 3 there is a simple example of this situation. In the initial triangulation there are 42 nodes but after all identifications only 26 distinct nodes remain. We have used FreeFEM to triangulate the subdomains [17]. Note that when triangulating it is useful to have a triangulation which is almost uniform in the given metric. This can be done by giving the relevant metric to the triangulation algorithm [18]. In Figure 4 there is an example where the

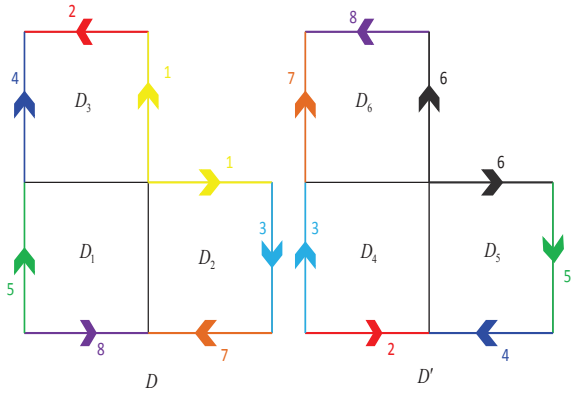

Fig. 2: The construction of the sphere using the maps φ_ℓ. The arrows indicate the orientation of the boundary used in the identification.

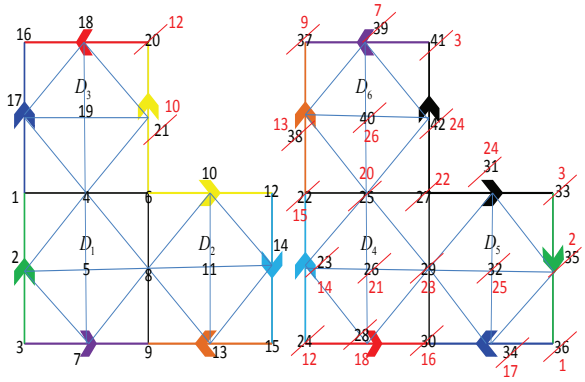

Fig. 3: A simple mesh which shows the original numbering of the nodes as well as the numbering after all appropriate identifications.

triangulation is far from uniform in the standard metric but almost uniform in the relevant metric of the surface.

Having constructed the triangulation we compute the relevant integrals in (13) and (14) in the standard way. Finally in assembling the resulting global matrices we have to take into account the identifications indicated in Figures 2 and 3. We have implemented our code for P_1 and P_2 elements.

4.4 Explicit construction of various surfaces

Let us next describe one convenient way to define a large class of maps Φ^t which we use in the examples given later. Let us for the moment suppress the time dependence and

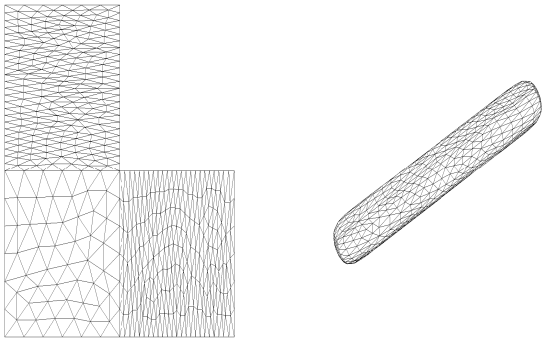

Fig. 4: On the left the triangulations of the subdomains and the resulting triangulation of the surface. Since the relevant metric was taken into account in the triangulation of the subdomains the resulting triangulation on the surface is almost uniform.

consider a single diffeomorfism Φ. Let $\rho : \mathbb{R}^3 \setminus \{0\} \to \mathbb{R}$ be a positive and a positively homogeneous function, i.e. $\rho(cx) = \rho(x)$ for all $c > 0$ and let us define a map $\Phi : S^2 \to \mathscr{S}$ by the formula $\Phi(x) = \rho(x)x$. Evidently $\mathscr{S}$ is a smooth surface which is a topological sphere and it is given by the equation $|x| = \rho(x)$. In this case we compute

$$\begin{aligned} d\Phi =& \rho I + x \otimes d\rho \quad \Rightarrow \\ d\Phi^T d\Phi =& \rho^2 I + \rho\left(x \otimes d\rho + d\rho \otimes x\right) + |x|^2 d\rho \otimes d\rho \end{aligned}$$

But we will always evaluate $d\Phi^T d\Phi$ on the unit sphere where $|x|^2 = 1$. Moreover the columns of $d\varphi_j$ are tangent to the unit sphere which implies that $d\varphi_j^T x \otimes d\rho = 0$ and $d\rho \otimes x\, d\varphi_j = 0$. Hence

$$\begin{aligned} \hat{G}_j =& d\varphi_j^T d\Phi^T d\Phi d\varphi_j = \rho^2 d\varphi_j^T d\varphi_j + d\rho\, d\varphi_j \otimes d\rho\, d\varphi_j \\ =& \rho^2 G_j + d\rho\, d\varphi_j \otimes d\rho\, d\varphi_j \end{aligned}$$

We will consider 2 different kinds of ρ in the examples below. To obtain a surface of revolution one can choose

$$\rho = \rho_1 \circ \xi_1 \quad \text{where} \quad \xi_1(x) = \frac{x_3}{|x|} \tag{16}$$

and $\rho_1 : [-1,1] \to \mathbb{R}$ is the function which gives the profile of the surface. The metric in this case is given by

$$\hat{G}_j = \rho_1^2(x_3) G_j + (\rho_1'(x_3))^2 \left(d\xi_1\, d\varphi_j \otimes d\xi_1\, d\varphi_j\right) \quad \text{where}$$

$$d\xi_1 = \left(-x_1 x_3, -x_2 x_3, x_1^2 + x_2^2\right)$$

Recall that everything is evaluated on the unit sphere.

To construct a more general surface we can choose

$$\rho = \rho_2 \circ \xi_2 \quad \text{where}$$
$$\xi_2 = \Big(\frac{x_1}{\sqrt{x_1^2+x_2^2}}, \frac{\sqrt{x_1^2+x_2^2}}{|x|} \Big) \tag{17}$$

Now it may appear that ρ is not well defined because ξ_2 is not defined on the x_3 axis. However, this is easy to arrange by choosing a suitable ρ_2. In particular we consider only polynomial maps

$$\rho_2(y) = \sum_\alpha c_\alpha y^\alpha$$

where α is a multi index and $\alpha_1 \le \alpha_2$. In this case the resulting map ρ is smooth and the metric can now again be written as

$$\hat{G}_j = \rho^2 G_j + d\rho\, d\rho \otimes d\rho\, d\rho$$

There are of course many ways to introduce time dependence to the problem. One relatively straightforward and natural way is to use a linear homotopy. We define the initial shape by ρ_{init} and the final shape by ρ_{fin} and set

$$\rho_{\mathsf{H}}(x,t) = \big(1-\zeta(t)\big)\,\rho_{\mathsf{init}} + \zeta(t)\,\rho_{\mathsf{fin}} \tag{18}$$

Here ζ is a function with the following properties: (i) $\zeta(0)=0$, (ii) $\zeta'(t) \ge 0$ and (iii) $\lim_{t\to\infty}\zeta(t) = 1$.

In biological context it is rather natural to take ρ_{init} as the constant map, or at least quite close to constant. The map ρ_{fin} should then give the shape of the organism as an adult and consequently it must be quite complicated in realistic cases. We do not attempt to go so far as to model a specific species but anyway we feel that the examples below are at least suggestive of biological shapes. Anyway when ρ_{init} is constant we can write the time dependent metric as

$$G_j^t = \rho_H^2 G_j + \zeta^2\, d\rho_{\mathsf{fin}}\, d\varphi_j \otimes d\rho_{\mathsf{fin}}\, d\varphi_j \tag{19}$$

5 Numerical results

In all cases below we have used P_1 finite elements in the computations and the initial condition was taken as a small random perturbation of the constant solution (8). In Figures red corresponds to large and blue to small values of the solution. In all computations the solution stayed positive for the time-steps we used. Also computations were stable for these time-steps. In other words choosing a time-step which seems reasonable from the point of view of accuracy always produced stable and positive solutions.

Table 1: Parameters used for the the surface given by (20).

d_1	d_2	γ	a	b	q_0	L_0	α	β	r	k	p
1	100	500	0.1	0.9	0.1	0.5	0.8	0.3	0.5	0.5	5

5.1 A simple surface

Let us first consider the surface which was studied in [2]. The equation of the surface is given by

$$x_1^2 + x_2^2 + q^2 \Big(\frac{x_3}{L}\Big)^{4p} = q^2 \tag{20}$$

Here p is constant but q and L depend on time:

$$q = q_0\big(1+\alpha(1-e^{-kt})\big)$$
$$L = \frac{L_0}{\beta + (1-\beta)e^{-rt}}$$

One can check that this gives a nice family of surfaces according to Definition 3.3. The relevant parameters for the surface and the Schnakenberg model are given in Table 1. We have chosen the parameter values which were used in [2]. Using these parameters we have $I_{\mathsf{crit}} \approx (0.013, 0.78)$ and initially there are 16 unstable modes: $\lambda_j/\gamma \in I_{\mathsf{crit}}$ for $1 \le j \le 16$.

Initially the surface is a short "snake" which then becomes longer and a bit thicker as the time goes by. Since the shape of this surface is so close to a sphere this is easiest to parametrize by modifying directly our basic maps in (15). The relevant maps are given by

$$\begin{aligned}
\varphi_1^t &= \gamma_1^{-1/2}\begin{pmatrix} qz_1 \\ qz_2 \\ \gamma_1^{1/2-1/4p}L \end{pmatrix}, \\
\varphi_2^t &= \gamma_2^{-1/2}\begin{pmatrix} q \\ qz_2 \\ \gamma_2^{1/2-1/4p}L(2-z_1) \end{pmatrix} \\
\varphi_3^t &= \gamma_3^{-1/2}\begin{pmatrix} qz_1 \\ q \\ \gamma_3^{1/2-1/4p}L(2-z_2) \end{pmatrix} \\
\gamma_1 &= 1+z_1^2+z_2^2\,, \\
\gamma_2 &= 1+(z_1-2)^{4p}+z_2^2\,, \\
\gamma_3 &= 1+z_1^2+(z_2-2)^{4p}
\end{aligned} \tag{21}$$

Then we set $\varphi_{j+3}^t = -\varphi_j^t$ as usual. The formula for the metric is quite messy so we will not give it explicitly but it is anyway quite straightforward to program.

The triangulation used in the computation is shown in Figure 4. In Figure 5 there are solutions at two time

instants. The solution approaches rather quickly a stationary solution. This seems rather natural because there are initially already many unstable modes so one expects the evolution to be quite rapid and indeed already at $t = 1.6$ the solution is quite far from constant.

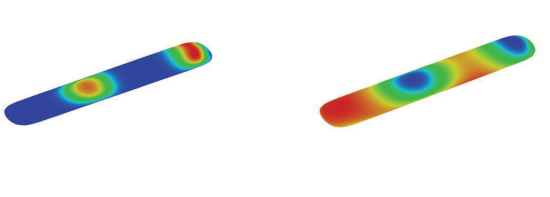

(a) On the left $0.1 \leq u_1 \leq 7.08$ and on the right $0.16 \leq u_2 \leq 0.66$.

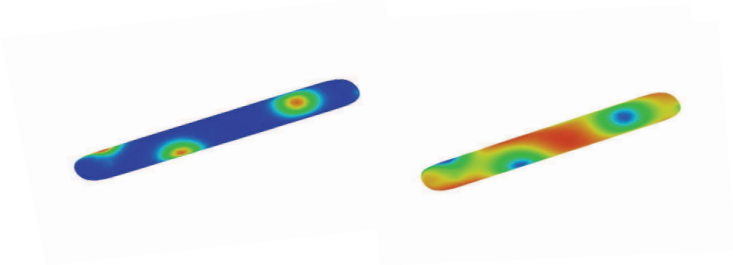

(b) On the left $0.09 \leq u_1 \leq 8.11$ and on the right $0.14 \leq u_2 \leq 0.59$.

Fig. 5: On the first row there are solutions u_1 and u_2 at $t = 1.6$ and on the second at $t = 2.75$.

Let us then consider another case where we can illustrate the role of eigenfunctions to the resulting patterns. Using the parameters given in Table 2 we have $I_{\text{crit}} \approx (0.17, 0.43)$. In this case there are initially no unstable modes. However, at $t = 1.6$ we have $\lambda_2/\gamma \in I_{\text{crit}}$ and in Figure 6 there is the corresponding eigenfunction as well as the solution to the problem. The patterns are almost identical.

In general we could say that when the surface grows the eigenvalues tend to move to the left. Hence if there are no unstable modes initially the solution is likely to be characterized by the eigenfunction corresponding to the first λ_j/γ which enters the critical interval from the right. Recall that for general surfaces the eigenvalues are simple so it is possible to have so clear a correspondence as in Figure 6. On the other hand in the atypical case of the sphere where there are high multiplicities of eigenvalues this sort of phenomenon is not likely.

Let us also recall that the eigenfunctions of the Laplacian are always orthogonal (4). This implies that the eigenfunctions corresponding to larger eigenvalues

Table 2: Another set of parameters for surface (20).

d_1	d_2	γ	a	b
1	20	72	0.2	1.0

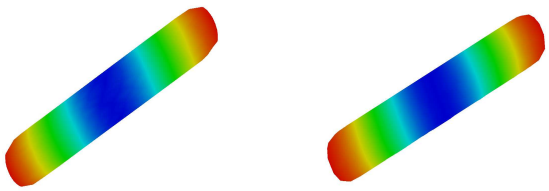

Fig. 6: On the left the eigenfunction corresponding to the eigenvalue λ_2 of the Laplacian on the surface (20) at $t = 1.6$. On the right the solution u_1 at $t = 1.6$. where $a = 0.2$, $b = 1$, $d_1 = 1$, $d_2 = 20$ and $\gamma = 72$.

oscillate more and more. Hence the final solutions corresponding to large γ tend to have finer patterns than the solutions with small γ.

Note again that the value of γ has no intrinsic meaning, only the value of γ relative to the size of the surface. Recall finally that according to Theorem 3.2 the solution tends to a constant solution if the first nonzero eigenvalue is too big. Hence the emergence of patters is impossible if the surface is too small and in this way the growth of the surface is essential to the emergence of patterns.

5.2 Surface of revolution

Let us then consider the final surface $\rho_{\text{fin}} = \rho_1 \circ \xi_1$ as in (16) where

$$\rho_1(s) = 1 + 3s^2 - 2s^3 \tag{22}$$

When we evaluate on the unit sphere we obtain

$$\begin{aligned} \rho_{\text{fin}} &= 1 + 3x_3^2 - 2x_3^3 \\ d\rho_{\text{fin}} &= 6x_3(1 - x_3)\left(-x_1x_3\,, -x_2x_3\,, 1 - x_3^2 \right) \end{aligned}$$

Using the linear homotopy (18) and choosing $\rho_{\text{init}} = 1$ and $\zeta(t) = 1 - e^{-3t}$ we can compute the metric by the formula (19). Choosing parameters as shown in Table 3 we have the critical interval $I_{\text{crit}} \approx (0.15, 0.55)$. Now initially we have the unit sphere so that according to (1) we have $\hat{\lambda}_3/\gamma$, $\hat{\lambda}_4/\gamma \in I_{\text{crit}}$ and there are thus initially 16 unstable modes.

Table 3: Parameters for surface (22).

d_1	d_2	γ	a	b
1	10	50	0.1	0.8

Table 4: Parameters for surface (23)

d_1	d_2	γ	a	b
10	90	10	0.1	0.8

In Figure 7 there are solutions for some time instants. There were 2890 nodes in the mesh and we used $\delta t = 0.1$ as the time-step. Since there are already initially some unstable modes the solution stabilizes quite fast. For the final surface there are 127 unstable modes since $\lambda_j/\gamma \in I_{\text{crit}}$ for $56 \leq j \leq 182$.

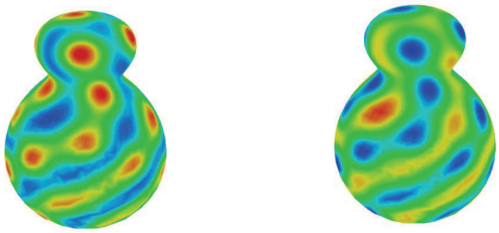

(a) On the left $0.18 \leq u_1 \leq 1.79$ and on the right $0.59 \leq u_2 \leq 1.39$

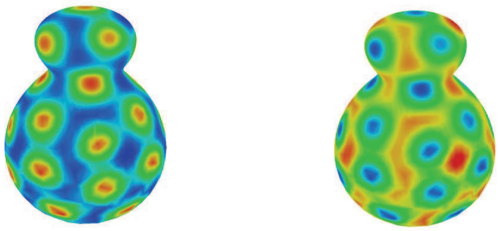

(b) On the left $0.29 \leq u_1 \leq 2.02$ and on the right $0.52 \leq u_2 \leq 1.29$

Fig. 7: On the first row u_1 and u_2 at $t = 10$. On the second row u_1 and u_2 at $t = 30$.

5.3 More complicated surface

Let us now consider the case where $\zeta(t) = 1 - e^{-t}$, $\rho_{\text{init}} = 1$ and the final surface is given by $\rho_{\text{fin}} = \rho_2 \circ \xi_2$ where ξ_2 is as in (17) and

$$\rho_2 = (3 + 2y_1y_2)\big(4 + 3y_2^5(16y_1^5 - 20y_1^3 + 5y_1)\big) \qquad (23)$$

When evaluated on the unit sphere we have

$$\rho_{\text{fin}} = \big(3 + 2x_1\big)\big(4 + 3x_1^5 - 30x_1^3x_2^2 + 15x_1x_2^4\big)$$

In Figure 8 there are solutions for some time instants. In this case there were 2756 nodes in the mesh and the time-step was $\delta t = 0.1$. The parameters were chosen as in Table 4 and the critical interval is $I_{\text{crit}} \approx (0.018, 0.051)$. In this case there are initially no unstable modes so it is natural that it takes a long time before patterns start to emerge and the even more before the solution settles. For the final surface we have 97 unstable modes since $\lambda_j/\gamma \in I_{\text{crit}}$ for $52 \leq j \leq 148$.

6 Conclusion

We have formulated the Schnakenberg model on the evolving surface and computed the solution in various cases when the surface is topologically a sphere. However, our approach can also be used to other types of surfaces, as long as the topological type of the surfaces remains the same during the computation. Our method of computation allows a very flexible way to define appropriate families of surfaces. Our code can also be adapted to handle similar nonlinear diffusion models.

Our approach is based on explicitly taking into account the changing Riemannian metric of the surface which makes all computations completely intrinsic. Hence we avoid all problems related to approximating surfaces as submanifolds of $\mathbb{R}^3$. In particular the mesh tangling which sometimes is problematic in moving grid type methods cannot arise in our framework.

In our method we use six coordinate patches to cover the whole sphere. Using spherical coordinates one could in principle use only one patch. However, this coordinate system is singular at the ”poles” which would lead to numerical difficulties. While it is perhaps possible to work around these difficulties the resulting scheme is necessarily somewhat ad hoc. Our coordinate systems are always numerically stable.

In the case of the sphere one could also try to use spherical harmonics in numerical approximation like in [5]. However, it is not clear how to extend this approach to more general surfaces. Indeed it was one of our goals to treat a large class of surfaces in a unified way.

We have also analyzed the role of the eigenfunctions of the Laplacian in the emergence of patterns and it seems that at least in some cases one can predict the overall nature of patterns simply by studying appropriate eigenvalues and eigenfunctions. These observations seem to be new.

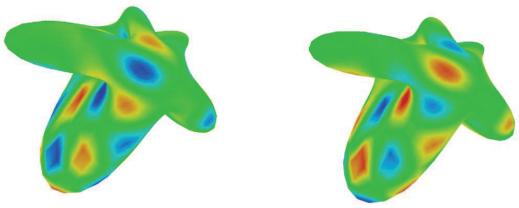

(a) On the left $0.84 \leq u_1 \leq 0.96$ and on the right $0.95 \leq u_2 \leq 1.01$. At this stage solution is still relatively close to constant.

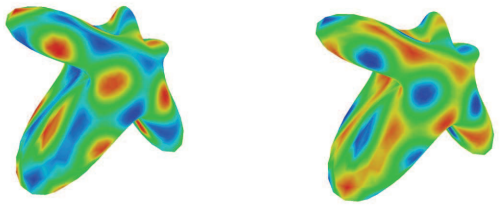

(b) On the left $0.33 \leq u_1 \leq 1.64$ and on the right $0.62 \leq u_2 \leq 1.26$.

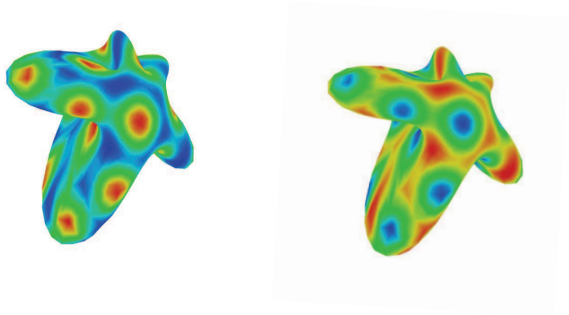

(c) On the left $0.38 \leq u_1 \leq 1.71$ and on the right $0.59 \leq u_2 \leq 1.24$.

Fig. 8: Concentration of u_1 and u_2 at $t = 10$, 30 and 70.

References

[1] J. D. Murray, Mathematical biology II, Volume 18, Springer-Verlag, 2003.

[2] R. Barreira and C. M. Elliott and A. Madzvamuse, The surface finite element method for pattern formation on evolving biological surfaces, J. Math. Biol. **63**(6), 1095-1119 (2011).

[3] D. Calhoun and C. Helzel, A finite volume method for solving parabolic equations on logically Cartesian curved surface meshes, SIAM J. Sci. Comput. **31**(6), 4066-4099 (2009/10).

[4] D. Calhoun and C. Helzel and R. LeVeque, Logically rectangular grids and finite volume methods for PDEs in circular and spherical domains, SIAM Rev. **50**(4), 723-752 (2008).

[5] M.A.J. Chaplain and I. G. Graham, Spatio-temporal pattern formation on spherical surfaces: numerical simulation and application to solid tumour growth, J. Math. Biol. **42**, 387-424 (2001).

[6] G. Dziuk, C. M. Elliott, Finite elements on evolving surfaces, IMA Juornal of Numerical Analysis **72**(2), 262-292 (2007).

[7] G. Dziuk and C. M. Elliott, Surface finite elements for parabolic equations, J. Comput. Math. **25**(4), 385-407 (2007).

[8] M. Sattari and J. Tuomela, On the numerical solution of elliptic and parabolic PDE in the real projective plane, submitted.

[9] M. Sattari and J. Tuomela and H. Niskanen and J. Hämäläinen, Coupled simulation of the spherical angles of rigid fibres by using a fibre orientation probability distribution model, Int. J. Multiphase Flow **65**, 61-67 (2014).

[10] A. Madzvamuse and P.K. Maini and A.J. Wathen, A moving grid finite element method for the simulation of pattern generation by Turing models on growing domains, J. Sci. Comp **24**(2), 247-262 (2005).

[11] J. Schnakenberg, Simple chemical reaction systems with limit cycle behaviour, J. Theoret. Biol. **81**(3), 389-400 (1979)

[12] J. M. Lee, Introduction to smooth manifolds, Graduate Texts in Mathematics, Volume 218, Springer-Verlag, New York, 2003.

[13] M. Berger, A panoramic view of Riemannian geometry, Springer-Verlag, Berlin, 2003.

[14] J. Marsden and T. Hughes, Mathematical foundations of elasticity, Dover Publications Inc., New York, 1994.

[15] M. Ghergu and V. Rădulescu, Nonlinear PDEs, Springer Monographs in Mathematics, Springer, Heidelberg, 2012.

[16] C. Venkataraman and O. Lakkis and A. Madzvamuse, Global existence for semilinear reaction-diffusion systems on evolving domains, J. Math. Biol. **64**(1-2), 41-67 (2012).

[17] F. Hecht, New development in freefem++, J. Numer. Math. **20**(3-4), 251-265 (2012).

[18] P. Frey and P.-L. George, Mesh generation, Application to finite elements, ISTE, London, 2008.

Mahdieh Sattari is a Ph.D student in applied mathematics at University of Eastern Finland. She is going to defend her PhD dissertation in autumn 2015. Her research interests are in applied mathematics including scientific computing and mathematical modeling in physics and biology.

Jukka Tuomela got his Ph.D. degree in mathematics from Université de Paris 7, Paris, France, in 1992. He is currently a Professor of Mathematics at the University of Eastern Finland, Joensuu, Finland. His research has been concerned with differential equations and their computational analysis.